RSC Mechanochemistry

ROYAL SOCIETY OF CHEMISTRY

PAPER

View Article Online
View Journal

Check for updates

Cite this: DOI: 10.1039/d4mr00127c

The cubic structure of Li_3As stabilized by pressure or configurational entropy *via* the solid solution Li_3As–Li_2Se†‡

Martin Schmid, Florian Pielnhofer and Arno Pfitzner *

Received 29th October 2024
Accepted 12th December 2024

DOI: 10.1039/d4mr00127c

rsc.li/RSCMechanochem

The hexagonal to cubic phase transition of Li_3As was investigated at high pressure and temperature, revealing a cubic high-pressure polymorph in the Li_3Bi structure type. This cubic structure type is preserved in the solid solution of Li_3As–Li_2Se synthesized *via* mechanochemical ball milling. The solid solutions were investigated *via* X-ray powder diffraction, showing a linear dependency of the lattice parameter *a* on the mole fraction of the boundary phases Li_3As and Li_2Se, according to Vegard's law. Configurational entropy is generated by mixed anion lattice occupation between arsenide and selenide and therefore stabilizes the cubic structure of the solid solution. At elevated temperatures, the solid solution of Li_3As–Li_2Se reveals an exsolution process by forming the boundary phases Li_3As and Li_2Se, proving the metastable character of the system. Impedance spectroscopy was used to determine the lithium-ion conductivities in the Li_3As–Li_2Se system, showing significantly higher conductivity values ($\sim 10^{-4}$ to 10^{-6} S cm^{-1} at 50 °C) compared to the pure end members Li_3As ($\sim 10^{-7}$ S cm^{-1} at 50 °C) and Li_2Se ($\sim 10^{-7}$ S cm^{-1} at 175 °C).

Introduction

For all binary lithium pnictogenides Li_3Pn (Pn = N, P, As, Sb, Bi), a cubic modification in the Li_3Bi structure type is mentioned in the literature; however, to the best of our knowledge, for the cubic modification of Li_3As, no experimental data are available in scientific publications.[1,2] In 2022, we reported lithium-ion mobility in Li_3As and calculated the phase stability of the cubic high-pressure modification *via* DFT (density functional theory).[3] Herein, we report experimental results on the cubic polymorph of Li_3As, *i.e.*, X-ray powder diffraction (XRPD) of a quenched sample obtained from high-pressure and high temperature conditions in a belt press. Thus, this missing part in the puzzle for Li_3Pn (Pn = N, P, As, Sb, Bi) is available now.

We further show that the pressure induced cubic structure of Li_3As can also be stabilized by the formation of a solid solution in the Li_3As–Li_2Se system. Two examples for solid solutions between binary lithium chalcogenides and lithium pnictogenides are known in the literature. Restle *et al.* reported a solid solution of Li_3N and Li_2O in a rigid open framework boron structure ($Li_6B_{18}(Li_3N)_{1-x}(Li_2O)_x$, $0 \leq x \leq 1$), since the authors claim that pristine Li_3N and Li_2O are not miscible in the solid state.[4,5] The second example for solid solutions of binary lithium chalcogenides and lithium pnictogenides was reported by Szczuka *et al.* in the Li_3P–Li_2S system, showing miscibility between the two phases in the range of $0.39 \leq x \leq 0.75$ (xLi_3P–$(1-x)Li_2S$).[6] The two boundary phases Li_2S and Li_3P crystallize in the cubic antifluorite structure type and the hexagonal Na_3As structure type, respectively. Despite the significant structural difference between Li_2S and Li_3P under ambient conditions, a solid solution in the antifluorite structure type is formed. The authors explain the miscibility by the fact that under pressure (4 GPa) Li_3P undergoes a hexagonal to cubic phase transition. Since the synthesis of the solid solution is carried out by high-energy ball milling of mixtures of Li_3P and Li_2S, the phase transition of Li_3P could be induced mechanochemically to form a cubic structure which is compatible with the cubic structure of Li_2S.[6] High temperature experiments reveal the decomposition of the solid solution into Li_3P and Li_2S at elevated temperatures (400–500 °C) indicating thermal stability of the solid solution only at lower temperatures.[6] Investigations on lithium-ion mobility show that the samples of the mixtures exhibit significantly higher lithium-ion mobility ($\sim 10^{-4}$ to 10^{-5} S cm^{-1}) than the boundary phases (Li_2S: 10^{-14} to 10^{-10} S cm^{-1}, Li_3P: 10^{-7} S cm^{-1}).[6–8]

Li_3Pn (Pn = N, P, As, Sb, Bi) compounds that adopt the cubic structure type under less extreme conditions are Li_3Sb and Li_3Bi. Li_3Bi indeed crystallizes in the cubic structure type under ambient conditions. In a detailed computational study, Hautier *et al.* discussed the potential application of Li_3Sb as a high-mobility p-type transparent conductor.[9] Furthermore, Li_3Sb

Institut für Anorganische Chemie, Universität Regensburg, Universitätsstraße 31, 93053 Regensburg, Germany. E-mail: Arno.Pfitzner@chemie.uni-regensburg.de

† Dedicated to Prof. Hans Jörg Deiseroth on the occasion of his 80th birthday.

‡ Electronic supplementary information (ESI) available. See DOI: https://doi.org/10.1039/d4mr00127c

and Li_3Bi have been theoretically predicted to be above-average thermoelectric materials.[10,11] The improved thermoelectric performance of Li_3Sb samples that transform to the cubic polymorph *via* ball milling was demonstrated by Snyder and Aldemir *et al.*[12]

In this work, we show that the system with the higher homologues (Li_3As–Li_2Se) has similar properties to the solid solution of Li_3P–Li_2S. X-ray powder diffraction data of ball milled samples with the stoichiometry of $Li_{3-x}As_{1-x}Se_x$ ($0.2 \leq x \leq 1$) confirm the formation of a solid solution in a cubic structure. Analogous to the Li_3P–Li_2S system, the formation of the solid solution in the Li_3As–Li_2Se system can be rationalized by the accessibility of the high-pressure modification of Li_3As *via* mechanochemical synthesis since high local temperature and pressure are involved during ball milling. Configurational entropy introduced by the cubic mixed anion lattice (As^{3-} and Se^{2-}) in the solid solution could stabilize its cubic structure. Enhancing phase stability by introducing high configurational entropy to a structure is well known for cations in high entropy oxides which have gained significant interest over the recent decade.[13–15] However, stabilizing entropic contributions from anions are rarely mentioned in the literature. With the multi-anionic and -cationic oxofluoride $Li_x(Co_{0.2}Cu_{0.2}Mg_{0.2}Ni_{0.2}Zn_{0.2})OF_x$, Wang *et al.* showed the stabilizing entropic effect originating from the mixed anion lattice (O^{2-}/F^-) revealing promising properties for use as a cathode material in lithium-ion batteries.[16]

Results and discussion

The cubic high-pressure modification of Li_3As

For the cubic to hexagonal phase transition of Li_3As, Beister *et al.* reported a pressure of 4.5 GPa, but apart from the conversion pressure, no further information or experimental data was published.[2]

In this work we present the synthesis of the cubic structure of Li_3As by applying high-pressure (3.6 GPa) and high temperature (1350 °C) on a phase pure sample of hexagonal Li_3As (Na_3As structure type) using a belt press. XRPD was performed on a quenched sample. The powder diffraction pattern in Fig. 1 reveals high intensities of the cubic phase of Li_3As, which was indexed and refined (see the ESI‡) with a profile function, leading to the lattice parameter $a = 6.214(1)$ Å. Indexing and refinement of the cubic phase was performed based on the Li_3Bi structure type with the space group $Fm\bar{3}m$ (no. 225). The corresponding calculated diffraction profile of the cubic structure model shows perfect agreement with the measured diffraction pattern (Fig. 1). Previous DFT modelling by our group on the phase stability of Li_3As under high-pressure conditions predicted the cubic phase of Li_3As in the Li_3Bi structure type with the lattice parameter $a = 6.1909$ Å which differs only by 0.4% from the experimental data.[3] These findings confirm a hexagonal to cubic phase transition (α-Li_3As → β-Li_3As) at high pressure and high temperature for the compound under study (Fig. 2). The still pronounced reflections of hexagonal α-Li_3As (36%) prove that the hexagonal to cubic phase transition is not completed under the applied conditions. The cubic modification of Li_3As could be stabilized after quenching the sample from high pressure and high temperature to ambient conditions. Quenching is crucial to prevent the reverse cubic to hexagonal phase transition, which is observed during slow pressure and temperature reduction to ambient conditions. A similar behavior was found for the related compound Li_3P by Leonova *et al.*[17] *In situ* XRPD measurements under decreasing pressure from high to ambient pressure reveal the reverse cubic to hexagonal phase transition for Li_3P.[17] The heavier homologue Li_3Sb also behaves similarly, although the cubic structure is

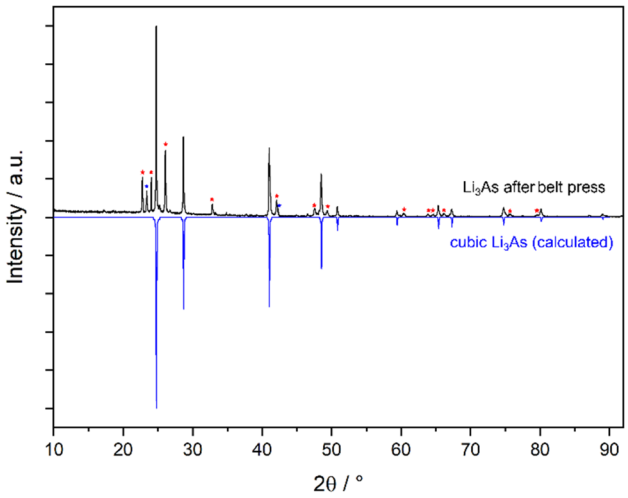

Fig. 1 Powder diffractogram of Li_3As after quenching from high-pressure and temperature to ambient conditions (black). Intensities marked with red stars can be assigned to hexagonal Li_3As (~36%). The intensity marked in blue cannot be assigned to any phase. Negative intensities show the calculated cubic Li_3As modification in the space group $Fm\bar{3}m$ (no. 225) with lattice parameters determined from the measured diffractogram.

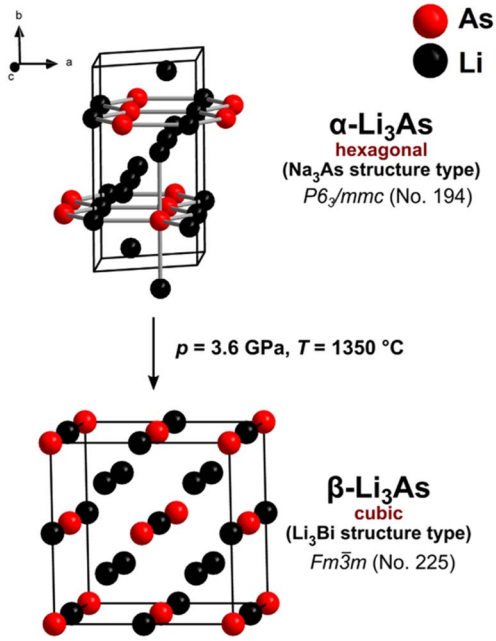

Fig. 2 Scheme of the hexagonal to cubic phase transition of Li_3As at 3.6 GPa and 1350 °C.

adopted after ball-milling, independent of the starting material (from the elements or transformation from hexagonal Li_3Sb). Thus, the application of high pressure forces the phase transformation of Li_3Sb at ambient temperature,[12] while additional high temperature is necessary for Li_3As. A minimal amount of the cubic polymorph already forms at 700 °C (Fig. S4‡). Furthermore, the metastable nature of the cubic polymorph of Li_3Sb was proven by annealing the cubic samples, which then transformed to the hexagonal phase.[12]

The solid solution in the Li_3As–Li_2Se system

In the ternary Li–As–Se system, the phases Li_2Se,[18] LiAs,[19] Li_3As,[20] Li_3As_7,[21] As_4Se_3,[22] As_4Se_4,[23] As_2Se_3,[24] $AsSe_2$,[25] and $LiAsSe_2$ [26] are known (Fig. 3). The solid solution $Li_{3-x}As_{1-x}Se_x$ ($0.2 \leq x \leq 1$) is highlighted in red in Fig. 3 between the two binary phases Li_3As and Li_2Se.

Synthesis and structure

Since the solid solution in the Li_3As–Li_2Se system was not accessible *via* classical solid-state reaction, it was realized by mechanochemical synthesis of the corresponding elements *via* ball milling. Ten samples in steps of $x = 0.1$ between Li_3As and Li_2Se ($Li_{3-x}As_{1-x}Se_x$) were synthesized. To obtain phase pure samples, the number of ball milling cycles (5 minutes of milling followed by 4 minutes of sample equilibration) was adjusted in the range of 12 to 36, since higher proportions of Li_3As need more mechanochemical treatment (higher energy input) to form a solid solution with Li_2Se. In Fig. 4 all powder diffractograms of the prepared samples are shown depending on their composition. Since samples with a stoichiometric ratio of 1 : 9 for $Li_3As : Li_2Se$ (equivalent to $x = 0.1$) show no significant formation of the cubic phase after several ball milling cycles, it is concluded that a miscibility gap is present near Li_3As in the solid solution with Li_2Se. Nevertheless, in the range of $0.2 \leq x \leq 1$ ($Li_{3-x}As_{1-x}Se_x$), all samples show XRPD pattern profiles originating from Li_2Se, which shift to lower 2θ values with increasing mole fractions of Li_3As. The cubic lattice parameter a of all samples including pure Li_2Se and the cubic modification of Li_3As was obtained from the corresponding diffraction patterns (Table S1‡) and plotted against the mole fraction x, as shown in Fig. 5. The lattice parameters of the solid solution show a Vegard-like trend, since the experimentally determined

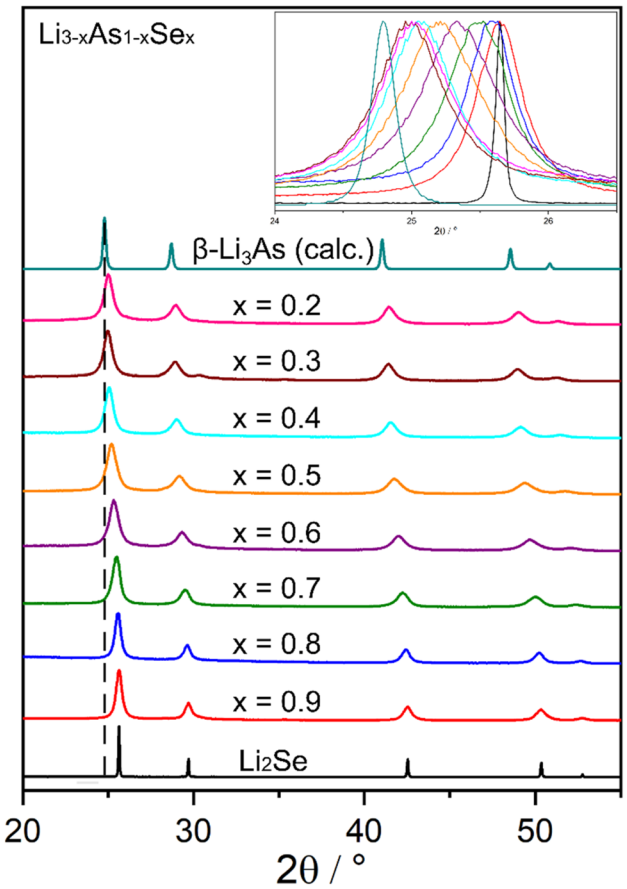

Fig. 4 Powder diffractograms of the solid solution $Li_{3-x}As_{1-x}Se_x$ ($0.2 \leq x \leq 1$). The powder diffractogram of β-Li_3As was calculated.

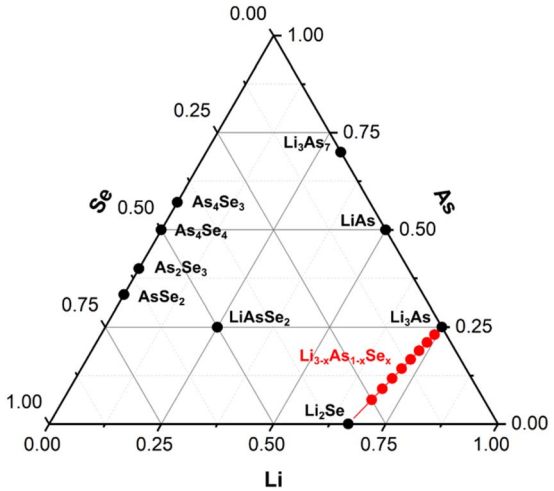

Fig. 3 Ternary phase diagram of the Li–As–Se system. The solid solution $Li_{3-x}As_{1-x}Se_x$ ($0.2 \leq x \leq 1$) is displayed in red.

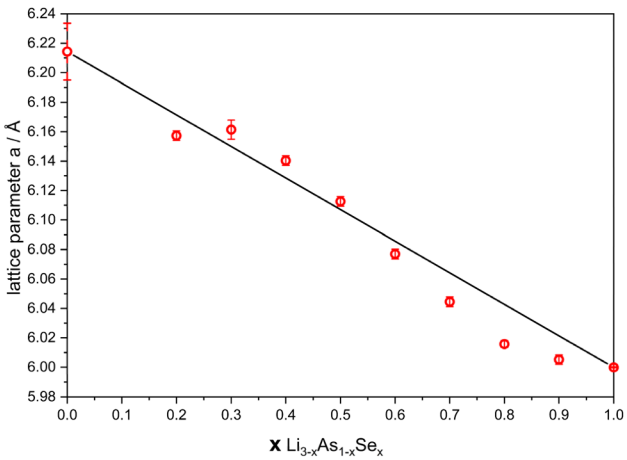

Fig. 5 Lattice parameter a plotted against the mole fraction x of the solid solution $Li_{3-x}As_{1-x}Se_x$ ($0.2 \leq x \leq 1$).

values exhibit deviations of less than 0.5% from the arithmetic mean of the lattice parameters from β-Li_3As and Li_2Se.[27] The small deviations, however, can be attributed to minimal amounts of oxygen in the samples, incomplete reactions or reactions with the container material, although these cannot be quantified.

Therefore, the stoichiometric compositions of the samples correspond with the lattice parameter *a* and the structure of the solid solution can be described as a cubic closed packing of arsenide and selenide ions forming a mixed occupancy site (Fig. 6). The tetrahedral voids are fully occupied with lithium cations and the octahedral voids are partly filled with lithium cations depending on the arsenide : selenide ratio of the anions, since the arsenic anions carry a higher negative charge.

Since Li_3As (hexagonal) and Li_2Se (cubic) differ in their crystal systems under ambient conditions, complete miscibility of both phases should not be possible in the solid state. Nevertheless, a solid solution is formed and a similar behavior has been reported for the lighter homologues in the Li_3P (hexagonal) and Li_2S (cubic) systems.[6] This can be rationalized by the fact that Li_3As and Li_3P possess a cubic high-pressure modification, which may become accessible during the ball milling process. In the presence of Li_2Se a metastable solid solution with the cubic high-pressure modification of Li_3As is formed. The formation of a solid solution series under the applied conditions (mechanochemical synthesis) can be rationalized by the smaller unit cell volume of the solid solution compared to the smaller combined unit cell volumes of the boundary phases Li_2Se and α-Li_3As as well as the gain in configurational entropy, which is generated by introducing selenide to the anion lattice of arsenide (Fig. 6). The free mixing energy (ΔG_{mix}) for a solid solution is defined as the sum of the mixing enthalpy (ΔH_{mix}) and the mixing configurational entropy (ΔS_{mix}).[28] The mixing enthalpy (ΔH_{mix}) can be further described as the sum of the inner energy (ΔU_{mix}) and the product of the applied pressure (p) and the change in the volume (ΔV_{mix}):

$$\Delta G_{mix} = \Delta U_{mix} + p\Delta V_{mix} - T\Delta S_{mix} \quad (1)$$

ΔV_{mix} is negative because the unit cell volume of the solid solution is smaller than the combined unit cell volumes of the boundary phases Li_2Se and Li_3As. This is because the cubic modification of Li_3As in the solid solution has a smaller unit cell volume than its hexagonal polymorph. Additional local high-pressure applied *via* mechanochemical synthesis results in an increased negative contribution to ΔG_{mix} and therefore favors the formation of the cubic solid solution. Secondly, elevated temperatures in the mechanochemical synthesis favor the presence of configurational entropy (ΔS_{mix}), which can be calculated by taking the mole fractions of arsenide (x_{As}) and selenide (x_{Se}) into account:[28]

$$\Delta S_{mix} = -R(x_{As} \ln x_{As} + x_{Se} \ln x_{Se}), \quad (2)$$

where R (J K^{-1} mol^{-1}) is the gas constant.

This gain in entropy leads to a higher free energy (negative ΔG_{mix}) for the solid solution of Li_3As–Li_2Se compared to the pristine compounds Li_3As and Li_2Se and stabilizes the cubic phase. Hence the cubic structure of Li_3As can be stabilized by a sufficient degree of heterovalent substitution in the anion lattice.

Thermodynamic stability of the solid solution

Thermal properties of the Li_3As–Li_2Se system were investigated by annealing $Li_{2.6}As_{0.6}Se_{0.4}$ samples to temperatures ranging from 200 °C to 700 °C for one week. Fig. 7 shows no change in the reflection profile up to a temperature of 300 °C, indicating phase stability. At 400 °C, the powder diffractogram shows complete decomposition (exsolution) of the solid solution into hexagonal Li_3As and Li_2Se revealing the metastable character of the solid solution. Similar findings have been reported for the Li_3P–Li_2S system, where powder diffraction data display the exsolution of the solid solution into Li_3P and Li_2S in the temperature range of 400 °C to 500 °C.[6] The thermodynamic instability of the solid solution at elevated temperatures indicates that the phases synthesized through mechanochemical methods are only kinetically stable under ambient conditions and decompose when energy (heat) is introduced to the system. This confirms the assumption that the synthesis conditions during the ball milling process must exceed ambient pressure and temperature since the solid solution is not accessible *via* classical solid state synthesis at elevated temperatures. At 700 °C, the two most intense reflections of Li_2Se broaden and shift to lower 2θ values accompanied by an intensity decrease of Li_3As compared to the XRPD data at 600 °C. These two observations suggest that after annealing the sample to 700 °C, some quantities of Li_3As remain incorporated in a solid solution with Li_2Se, indicating an increase in the phase stability of the solid

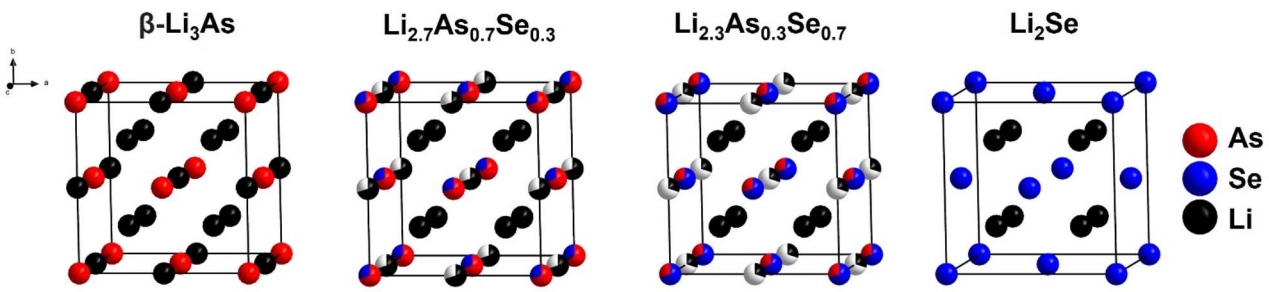

Fig. 6 Structural progression of the solid solution in the system $Li_{3-x}As_{1-x}Se_x$ ($0.2 \leq x \leq 1$) with the parent compounds β-Li_3As and Li_2Se.

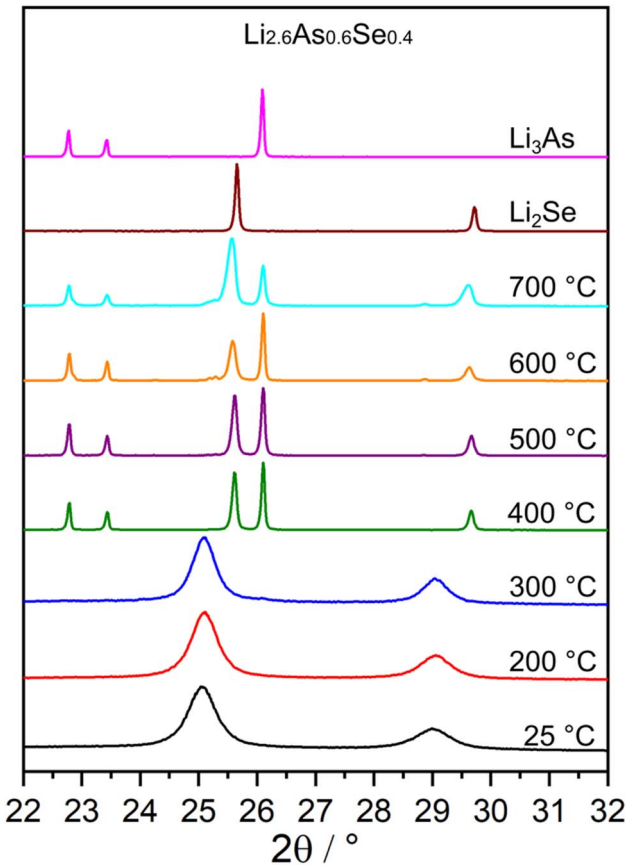

Fig. 7 Powder diffractograms of the $Li_{2.6}As_{0.6}Se_{0.4}$ compound after annealing to the displayed temperatures for one week and powder diffractograms of the end members Li_3As (hexagonal) and Li_2Se.

solution. This finding may be thermodynamically explained since the free mixing energy of solid solutions at high temperatures and constant pressure is predominantly determined by the additional configurational entropy ($\Delta G_{mix} = \Delta U_{mix} + p\Delta V_{mix} - T\Delta S_{mix}$) of the arsenide/selenide lattice and therefore phase stability of the solid solution at temperatures above 700 °C might be possible. However, further investigations at higher temperatures were not performed, because the quartz tubes were already severely damaged after heat treatment at 700 °C. DTA of $Li_{2.6}As_{0.6}Se_{0.4}$ (Fig. S2‡) shows one endothermic peak in the two heating cycles (478 °C and 486 °C) and one exothermal peak in the two cooling cycles (469 °C and 470 °C), which can be assigned to melting and recrystallisation processes, since the formation of a regulus was observed. Additionally, XRPD of the analyzed sample reveals the presence of Li_3As and LiAs after DTA and the XRPD pattern of the cubic solid solution is shifted to higher 2θ values, indicating a lower mole fraction of Li_3As in the solid solution after DTA (Fig. S3‡). Both findings combined indicate a partial decomposition process of the solid solution during the DTA into hexagonal Li_3As and LiAs, forming a Li_2Se-richer solid solution. The annealed samples, as shown in Fig. 7, confirm the thermal instability of the solid solution above 400 °C. Additionally, since the cubic structure of Li_3As is not stable under these conditions, the exsolution of arsenide anions from the solid solution is plausible.

Impedance spectroscopy

AC impedance spectroscopy with ion blocking electrodes (indium) was performed to investigate the lithium-ion mobility in the solid solution in the Li_3As–Li_2Se system. For the phases $Li_{2.2}As_{0.2}Se_{0.8}$, $Li_{2.4}As_{0.4}Se_{0.6}$, $Li_{2.6}As_{0.6}Se_{0.4}$ and $Li_{2.8}As_{0.8}Se_{0.2}$ Nyquist plots (Fig. S5‡) were recorded in the temperature range from 50 to 100 °C in steps of 10 °C. Impedance spectra were fitted with an equivalent circuit (Table S4‡) and the resulting resistance values were used to calculate the specific ion conductivities of the samples (Table S2‡). In Fig. 8 the specific ion conductivities of the homogeneous solid solutions in the Li_3As–Li_2Se system are displayed in an Arrhenius plot. Activation energies (E_a) are given in Table S5.‡ Higher lithium-ion conductivities are observed with increasing content of As in the samples. Conductivity values at 50 °C of the solid solution range from 10^{-6} S cm^{-1} for $Li_{2.2}As_{0.2}Se_{0.8}$ to 10^{-4} S cm^{-1} for $Li_{2.8}As_{0.8}Se_{0.2}$ with an activation energy of approximately 0.45 eV (Table S2‡). This two-order-of-magnitude difference in lithium-ion conductivities can be explained by the increasing lithium-ion content in the octahedral voids along with the increasing As content. The higher charge carrier concentration in the octahedral voids therefore correlates with a higher overall lithium-ion conductivity. All measured ion conductivities in the Li_3As–Li_2Se system show significantly better lithium-ion mobility than the parent compounds Li_3As and Li_2Se. Our group previously reported a lithium-ion conductivity of about 10^{-7} S cm^{-1} for Li_3As (gold blocking electrodes) at 50 °C and herein we observed lithium-ion conductivities of about 10^{-7} to 10^{-5} S cm^{-1} (gold blocking electrodes) for Li_2Se in the temperature range of 175 to 300 °C (Fig. S5 and Table S3‡).[3] At lower temperatures, the lithium-ion conductivities of Li_2Se were not measured because the impedance exceeded the range of our setup. Nevertheless, Li_2Se exhibits significantly lower lithium-ion conductivity values compared to the corresponding solid

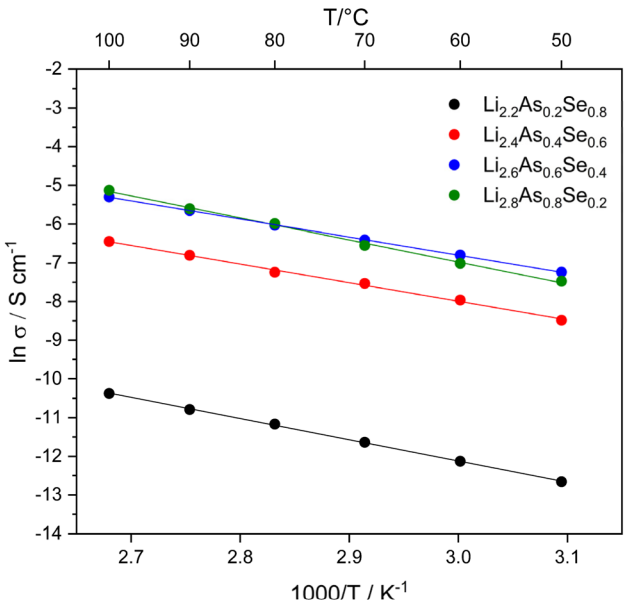

Fig. 8 Arrhenius plot of the solid solution $Li_{3-x}As_{1-x}Se_x$ ($0.2 \leq x \leq 1$).

solution. Similar findings have been reported for the closely related solid solution in the Li_3P–Li_2S system. For this system, impedance spectroscopy (lithium blocking electrodes) shows lithium-ion conductivities of 10^{-5} to 10^{-4} S cm^{-1} at room temperature, increasing with the P content, and these values are significantly higher compared to the binary phases Li_2S (10^{-14} to 10^{-10} S cm^{-1})[7,8] and Li_3P (10^{-7} S cm^{-1}).[6] However, the best Li ion conductors to date like $Li_{10}GeP_2S_{12}$ achieve conductivities up to 10^{-2} S cm^{-1},[29] which is not reached within the Li_3As–Li_2Se system.

Experimental

Because of the high air- and moisture-sensitivity of the compounds under discussion all manipulations were carried out in an argon-filled glovebox (M Braun) with oxygen and moisture levels less than 0.5 ppm. The materials must be handled with extreme caution, since the investigated compounds are highly toxic and reach high vapor pressures upon heating.

High-pressure synthesis

High-pressure experiments were performed in a belt apparatus according to the method described by *Range* and *Leeb* by using BN crucibles.[30] Samples of hexagonal Li_3As were pressed for 3 days at a temperature of 1350 °C and 3.6 GPa and were subsequently quenched to ambient conditions.

Synthesis

The samples in the Li_3As–Li_2Se system were prepared *via* ball milling (FRITSCH Pulverisette 7 premium line, 10 zirconia grinding balls (Ø = 10 mm), and 25 mL zirconia grinding bowls). Stoichiometric amounts (batch size: 2 g) of the elements Li (Merck, 99%), As (Chempur, sublimed) and Se (99.99%). 12 to 36 milling cycles (5 minutes of milling followed by 4 minutes of sample equilibration) at a rotation speed of 600 rotations per minute were performed to synthesize the compounds.

Powder diffraction

The powders of the samples were finely ground in an agate mortar, filled in quartz capillaries (Ø = 0.3 mm) and were subsequently flame sealed. The capillaries were placed on a STOE STADI P diffractometer (Stoe & Cie) equipped with a spinner, and a Mythen 1 K detector, using CuKα_1-radiation (λ = 1.5406 Å). Raw data were handled with the WinXPOW software package (Stoe & Cie).[31]

Differential thermal analysis (DTA)

Flame-sealed quartz tubes (Ø = 2 mm) filled with the reacted samples were measured using a SETARAM TG-DTA 92.16.18. Thermal analysis was carried out in the temperature range of 25 to 800 °C at a heating/cooling rate of 10 °C min^{-1}.

Impedance spectroscopy

AC impedance conductivity measurements were performed using a Zahner Zennium impedance analyzer. Temperature was controlled using an Eurotherm heating device. The whole setup was placed in a glovebox (M Braun) under an argon atmosphere. Impedance data were recorded in steps of 10 °C from 50–100 °C for frequencies of 1 MHz to 100 mHz. Active cooling is not possible with the setup in the argon-filled glovebox. Therefore, the temperature dependent series were started at 50 °C. The samples were cold pressed to pellets (Ø = 8 mm) and placed between pieces of indium foil which were in contact with platinum electrodes. The processing and fitting of the data were performed using the Zahner Analysis software package.[32]

Conclusions

We report the synthesis and characterization of the hexagonal (Na_3As structure type) to cubic (Li_3Bi structure type) phase transition of Li_3As at high temperature and high pressure. The cubic polymorph of Li_3As was obtained through heat and pressure treatment in a belt press followed by quenching to ambient conditions and characterization *via* XRPD.

Furthermore, we investigated the solid solution in the Li_3As–Li_2Se system stabilizing the cubic modification of Li_3As *via* configurational entropy by heterovalent substitution of the arsenide ions with selenide ions. The samples in the Li_3As–Li_2Se system were synthesized *via* ball milling of stoichiometric amounts of the corresponding elements. Powder diffraction data of the ball milled samples show miscibility of Li_3As and Li_2Se in the range of $0.2 \leq x < 1$ ($Li_{3-x}As_{1-x}Se_x$). The cubic lattice parameter of these samples follow Vegard's law.[27] The structure of the solid solution series can be described as a filled antifluorite structure type or alternatively as a deficient Li_3Bi structure type, *i.e.* arsenide and selenide ions occupy the anion positions of a fcc lattice. The tetrahedral voids therein are fully occupied by lithium cations. The octahedral voids are partly filled with the remaining lithium cations, as determined from the arsenide : selenide ratio. Despite the different crystal systems of Li_3As (hexagonal) and Li_2Se (cubic) under ambient conditions a solid solution is formed after mechanochemical synthesis. Since we have evidence for the cubic high-pressure modification of Li_3As, it is plausible to claim that cubic Li_3As is accessible *via* mechanochemical synthesis. We propose the formation of the solid solution during the ball milling process. The gain in configurational entropy (ΔS_{mix}) from mixing arsenide and selenide in the anion lattice along with the smaller volume (ΔV_{mix}) of the solid solution compared to the boundary phases can be regarded as the driving force for the formation of the cubic solid solution. Elevated local pressure and temperature in the mechanochemical synthesis amplify both influences on the free mixing energy ($\Delta G_{mix} = \Delta U_{mix} + p\Delta V_{mix} - T\Delta S_{mix}$), thus leading to the stabilization of the solid solution. The exsolution process of the solid solution at 400 °C into the boundary phases Li_3As and Li_2Se reveals the metastable character of the solid solution at elevated temperatures. Impedance spectroscopy shows high lithium-ion conductivity for Li_3As–

Li_2Se, ranging from about 10^{-4} to 10^{-6} S cm^{-1} at 50 °C, which is significantly higher than the conductivities of the parent compounds Li_3As and Li_2Se.[3]

Data availability

All data, *i.e.*, X-ray powder data, thermal analyses and impedance measurements are available from the authors on request.

Conflicts of interest

There are no conflicts to declare.

Acknowledgements

The authors express their gratitude to the Free State of Bavaria and the University of Regensburg for providing excellent working conditions and thank Ulrike Schieβl for DTA measurements.

References

1 H. J. Beister, K. Syassen and J. Klein, Phase Transition of Na_3As under Pressure, *Z. Naturforsch. B*, 1990, **45**, 1388–1392.
2 H. J. Beister, J. Klein, I. Schewe and K. Syassen, Structural phase transitions of alkali metal pnictides and chalkogenides, *High Press. Res.*, 1991, **7**, 91–95.
3 F. Wegner, F. Kamm, F. Pielnhofer and A. Pfitzner, Li_3As and Li_3P revisited: DFT modelling on phase stability and ion conductivity, *Z. Anorg. Allg. Chem.*, 2022, **648**, me202100358.
4 T. M. F. Restle, L. Scherf, J. V. Dums, A. G. Mutschke, R. J. Spranger, H. Kirchhain, A. J. Karttunen, L. van Wüllen and T. F. Fässler, Lithium-ion Mobility in $Li_6B_{18}(Li_3N)$ and Li Vacancy Tuning in the Solid Solution $Li_6B_{18}(Li_3N)_{1-x}(Li_2O)_x$, *Angew. Chem., Int. Ed.*, 2023, **62**, e202213962.
5 R. J. Spranger, H. Kirchhain, T. M. F. Restle, J. V. Dums, A. J. Karttunen, L. van Wüllen and T. F. Fässler, Mechanism of Li-Ion Migration in the Superionic Conducting Open-Framework Structure $Li_6B_{18}(Li_3N)_{1-x}(Li_2O)_x$ $(0 \leq x \leq 1)$, *J. Phys. Chem. C*, 2023, **127**, 1622–1632.
6 C. Szczuka, B. Karasulu, M. F. Groh, F. N. Sayed, T. J. Sherman, J. D. Bocarsly, S. Vema, S. Menkin, S. P. Emge, A. J. Morris and C. P. Grey, Forced Disorder in the Solid Solution Li_3P-Li_2S: A New Class of Fully Reduced Solid Electrolytes for Lithium Metal Anodes, *J. Am. Chem. Soc.*, 2022, **144**, 16350–16365.
7 Z. Lin, Z. Liu, N. J. Dudney and C. Liang, Lithium superionic sulfide cathode for all-solid lithium-sulfur batteries, *ACS Nano*, 2013, **7**, 2829–2833.
8 Y. Seino, T. Ota, K. Takada, A. Hayashi and M. Tatsumisago, A sulphide lithium super ion conductor is superior to liquid ion conductors for use in rechargeable batteries, *Energy Environ. Sci.*, 2014, **7**, 627–631.
9 V.-A. Ha, G. Yu, F. Ricci, D. Dahliah, M. J. van Setten, M. Giantomassi, G.-M. Rignanese and G. Hautier, Computationally driven high-throughput identification of CaTe and Li_3Sb as promising candidates for high-mobility p-type transparent conducting materials, *Phys. Rev. Mater.*, 2019, **3**, 034601.
10 K. Peng, Z. Zhou, H. Wang, H. Wu, J. Ying, G. Han, X. Lu, G. Wang, X. Zhou and X. Chen, Thermoelectric performance of binary lithium-based compounds: Li_3Sb and Li_3Bi, *Appl. Phys. Lett.*, 2021, **119**, 033901.
11 X. Yang, Z. Dai, Y. Zhao, J. Liu and S. Meng, Low lattice thermal conductivity and excellent thermoelectric behavior in Li_3Sb and Li_3Bi, *J. Phys.: Condens. Matter*, 2018, **30**, 425401.
12 M. Yahyaoglu, T. Soldi, M. Ozen, C. Candolfi, G. J. Snyder and U. Aydemir, Stress/pressure-stabilized cubic polymorph of Li_3Sb with improved thermoelectric performance, *J. Mater. Chem. A*, 2021, **9**, 25024–25031.
13 C. M. Rost, E. Sachet, T. Borman, A. Moballegh, E. C. Dickey, D. Hou, J. L. Jones, S. Curtarolo and J.-P. Maria, Entropy-stabilized oxides, *Nat. Commun.*, 2015, **6**, 8485.
14 A. Sarkar, Q. Wang, A. Schiele, M. R. Chellali, S. S. Bhattacharya, D. Wang, T. Brezesinski, H. Hahn, L. Velasco and B. Breitung, High-Entropy Oxides: Fundamental Aspects and Electrochemical Properties, *Adv. Mater.*, 2019, **31**, e1806236.
15 S. Senkale, M. Kamp, S. Mangold, S. Indris, L. Kienle, R. K. Kremer and W. Bensch, Multi-Method Characterization of the High-Entropy Spinel Oxide $Mn_{0.2}Co_{0.2}Ni_{0.2}Cu_{0.2}Zn_{0.2}Fe_2O_4$: Entropy Evidence, Microstructure, and Magnetic Properties, *Chem. Methods*, 2023, **3**, e202200043.
16 Q. Wang, A. Sarkar, D. Wang, L. Velasco, R. Azmi, S. S. Bhattacharya, T. Bergfeldt, A. Düvel, P. Heitjans, T. Brezesinski, H. Hahn and B. Breitung, Multi-anionic and -cationic compounds: new high entropy materials for advanced Li-ion batteries, *Energy Environ. Sci.*, 2019, **12**, 2433–2442.
17 M. E. Leonova, I. K. Bdikin, S. A. Kulinich, O. K. Gulish, L. G. Sevast'yanova and K. P. Burdina, High-Pressure Phase Transition of Hexagonal Alkali Pnictides, *Inorg. Mater.*, 2003, **39**, 266–270.
18 E. Zintl, A. Harder and B. Dauth, Gitterstruktur der Oxyde, Sulfide, Selenide und Telluride des Lithiums, Natriums und Kaliums, *Z. Elektrochem. Angew. Phys. Chem.*, 1934, **40**, 588–593.
19 D. T. Cromer, The crystal structure of LiAs, *Acta Cryst.*, 1959, **12**, 36–41.
20 G. Brauer and E. Zintl, Konstitution von Phosphiden, Arseniden, Antimoniden und Wismutiden des Lithiums, Natriums und Kaliums, *Z. Phys. Chem. B*, 1937, **37**, 323–352.
21 W. Hönle, J. Buresch, K. Peters, J. H. Chang and H. G. von Schnering, Crystal structure of the low-temperature modification of trilithium heptaarsenide, LT-Li_3As_7, *Z. Kristallogr. N. Cryst. Struct.*, 2002, **217**, 485–486.
22 T. J. Bastow and H. J. Whitfield, Crystal data and nuclear quadrupole resonance spectra of tetra-arsenic triselenide, *J. Chem. Soc., Dalton Trans.*, 1977, 959.
23 T. J. Bastow and H. J. Whitfield, Crystal structure of tetra-arsenic tetraselenide, *J. Chem. Soc., Dalton Trans.*, 1973, 1739.

24 A. C. Stergiou and P. J. Rentzeperis, The crystal structure of arsenic selenide, As_2Se_3, *Z. für Kristallogr. - Cryst. Mater.*, 1985, **173**, 185–191.
25 L. M. Lityagina, L. F. Kulikova, I. P. Zibrov, T. I. Dyuzheva, N. A. Nikolaev and V. V. Brazhkin, Structural transformations in the As–Se system under high pressures and temperatures, *J. Alloys Compd.*, 2015, **644**, 799–803.
26 T. K. Bera, J. I. Jang, J.-H. Song, C. D. Malliakas, A. J. Freeman, J. B. Ketterson and M. G. Kanatzidis, Soluble semiconductors $AAsSe_2$ (A = Li, Na) with a direct-band-gap and strong second harmonic generation: a combined experimental and theoretical study, *J. Am. Chem. Soc.*, 2010, **132**, 3484–3495.
27 L. Vegard, Die Konstitution der Mischkristalle und die Raumfllung der Atome, *Z. Phys.*, 1921, **5**, 17–26.
28 A. Sarkar, B. Breitung and H. Hahn, High entropy oxides: the role of entropy, enthalpy and synergy, *Scr. Mater.*, 2020, **187**, 43–48.
29 N. Kamaya, K. Homma, Y. Yamakawa, M. Hirayama, R. Kanno, M. Yonemura, T. Kamiyama, Y. Kato, S. Hama, K. Kawamoto and A. Mitsui, A lithium superionic conductor, *Nat. Mater.*, 2011, **10**, 682–686.
30 K.-J. Range and R. Leeb, Hochdruckmodifikationen der Lanthaniden(III)sulfide Ln_2S_3 (Ln = Lu-Ho, Y) mit U_2S_3-Struktur/High Pressure Modifications of the Rare Earth Sulfides Ln_2S_3 (Ln = Lu-Ho, Y) with U_2S_3-Structure, *Z. Naturforsch. B*, 1975, **30**, 889–895.
31 *STOE-WinXPOW, Vol. Version 3.0.2.5*, STOE & Cie GmbH, Darmstadt, 2011.
32 Zahner-Meßtechnik GmbH& Co. KG, Vol. Version Z.3.03, Thales-Flink, Kronach.

